Nonlinear Robust Adaptive Tracking Control of a Quadrotor UAV Via Immersion and Invariance Methodology

Bo Zhao, Bin Xian, *Senior Member, IEEE*, Yao Zhang, and Xu Zhang

***Abstract*—This paper presents a novel asymptotic tracking controller for an underactuated quadrotor unmanned aerial vehicle using the robust integral of the signum of the error (RISE) method and an immersion and invariance (I&I)-based adaptive control methodology. The control system is decoupled into two parts: the inner loop for attitude control and the outer loop for position control. The RISE approach is applied in the inner loop for disturbance rejection, whereas the I&I approach is chosen for the outer loop to compensate for the parametric uncertainties. The asymptotic tracking of the time-varying 3-D position and the yaw motion reference trajectories is proven via the Lyapunov-based stability analysis and LaSalle's invariance theorem. Real-time experiment results, which are performed on a hardware-in-the-loop simulation testbed, are presented to illustrate the performance of the proposed control scheme.**

***Index Terms*—Adaptive control, immersion and invariance (I&I), quadrotor, robust control, unmanned aerial vehicle (UAV).**

I. Introduction

OVER the past decades, the control of unmanned aerial vehicles (UAVs) has been a topic of considerable interest [1]. As a micro helicopter, the quadrotor UAV attracts great attention from military and civil applications due to its special advantages such as simple structure, vertical taking off and landing (VTOL), and rapid maneuvering. It has been widely used in a variety of situations including surveillance, fire fighting, environmental monitoring, and so on [2].

However, the control design for a quadrotor UAV is not a simple task. First of all, as a rotary-wing aircraft and an inherent nonlinear system, the quadrotor is open-loop instable, which requires a very fast control response and a large operation range [3]. Second, the quadrotor UAV has six degrees of freedom, but it has only four control inputs available; this is known as an underactuated property, which also leads to strong couplings between the dynamic states. Third, the value of some parameters associated with the dynamic model, such as the inertial moments and aerodynamic coefficients, cannot be measured or obtained exactly. Furthermore, the quadrotor UAV is very sensitive to external disturbances such as wind gust due to its small size and weight.

To solve these problems, different control techniques have been developed. Since the dynamic model of the quadrotor can be linearized, then some traditional linear control methods [4], [5] can be used to stabilize the quadrotor in a small range around the equilibrium. While considering the nonlinearity and a large operation range, the performance of the linear controller may be degraded. Thus, in recent years, more and more nonlinear robust control schemes have been developed.

As for the underactuated property, various control techniques have been developed for the quadrotor and other underactuated mechatronic systems, such as a wheeled mobile robot, an underwater vehicle, and overhead cranes [6], [7]. In [8], a novel robust backstepping-based controller that is based on an integral sliding-mode approach is proposed for an underactuated quadrotor. Although the design procedure of the backstepping scheme is very clear and the proof of the stability is standardized, the control gains are not easy for tuning. In [9], the dynamic system of the quadrotor is divided into the inner-loop and the outer-loop subsystem. Such scheme is not difficult for implementation, but the stability of the closed-loop system cannot be easily guaranteed. To overcome this drawback, an inner- and outer-loop-based flight controller is proposed in [10], and the asymptotic stability (AS) of the closed-loop system is proved via a theorem of cascaded systems.

To compensate for the parametric uncertainties, the adaptive nonlinear control method is a suitable choice and has been widely utilized [11]. However, the classic adaptive control method always requires a linear parameterization (LP) condition, and sometimes, the controller's singularities will come into being [12]. Recently, a new adaptive control design using the immersion and invariance (I&I) methodology is first proposed in [13] and then further developed by many researchers [14]–[17]. This approach, different from the classic adaptive method, does not require the LP condition, nor does it invoke certainty equivalence. It also simplifies the stability analysis by providing cross terms in the Lyapunov function [14]. In [15], an I&I method is used to estimate the unknown mass of a VTOL vehicle, and it guarantees that the estimation converges to its true value. In [16], to control a mini quadrotor UAV and overcome the uncertainties related with the thrust and drag coefficients, Fujimoto *et al.* simplified the dynamic model and developed an adaptive controller via the I&I methodology.

Manuscript received March 26, 2014; revised August 19, 2014; accepted September 30, 2014. Date of publication October 24, 2014; date of current version April 8, 2015. This work was supported by the Natural Science Foundation of Tianjin under Grant 14JCZDJC31900.

The authors are with the Institute of Robotics and Autonomous Systems, Tianjin Key Laboratory of Process Measurement and Control, School of Electrical Engineering and Automation, Tianjin University, Tianjin 300072, China (e-mail: xbin@tju.edu.cn).

Color versions of one or more of the figures in this paper are available online at http://ieeexplore.ieee.org.

Digital Object Identifier 10.1109/TIE.2014.2364982

However, only numerical simulation results are presented in these works, and no experimental results with the I&I adaptive design are provided. Apart from the control of UAV, I&I is also applied in visual servoing, control of pendulum on cart, and many other mechatronic systems [17].

Due to the existence of the external disturbances, much effort has been devoted to the design of a robust controller for a quadrotor. In [18], a general sliding-mode control (SMC) is developed for a class of uncertain underactuated systems and then utilized to stabilize a quadrotor helicopter. However, a drawback of the SMC is the chattering issue, which might deteriorate the control performance for practical implementation. To achieve a continuous control strategy, a robust integral of the signum of the error (RISE)-based controller is first presented in our previous work in [19] and further developed by other researchers [20]. The RISE feedback control can compensate for external disturbances and modeling uncertainties while ensuring semiglobal asymptotic results in the sense of a continuous control input. In [20], a control scheme using RISE feedback and neural network feedforward is applied on a rotorcraft-based UAV, and the semiglobal asymptotic tracking of the attitude and altitude states is proven by a Lyapunov-based stability analysis.

In this paper, in response to the aforementioned control difficulties for a quadrotor, a novel nonlinear robust tracking control scheme is proposed. First, to solve the underactuation and the couplings, the control system is divided into two parts: the inner-loop (attitude loop) controller and the outer-loop (position loop) controller. Second, to meet the requirements for robustness and fast response of attitude control, the RISE method is chosen to control the inner-loop subsystem. Finally, in order to address the unknown parameters and reduce the difficulty of control design, an I&I-based adaptive control scheme is utilized for the outer-loop subsystem control design. The proposed method yields the first I&I, RISE, and inner- and outer-loop-based control results for the underactuated quadrotor UAV in the presence of parametric uncertainties and unknown external disturbances. In particular, despite the difficulty of stability analysis for the inner/outer-loop approach, the proposed controller guarantees the asymptotic tracking of the closed-loop system via the Lyapunov-based stability analysis. Furthermore, to validate the performance of the proposed design, the nonlinear robust adaptive control design is verified by the real-time experiments on a hardware-in-the-loop simulation (HILS) quadrotor testbed. To our best knowledge, few previous works have demonstrated real-time experimental results for the I&I approach on a quadrotor UAV system.

This paper is organized as follows. The dynamic model of the quadrotor and the control objective is described in Section II. Section III details the control development, and in Section IV, the asymptotic tracking results are proven. Real-time experimental results are presented in Section V. Finally, some conclusion remarks are included in Section VI.

II. Problem Formulation

The schematic of a quadrotor UAV is shown in Fig. 1. The thrusts generated by the four rotors are denoted by $f_i(t)$, $i = 1, 2, 3, 4$, respectively. Let $\mathcal{I} = \{x_I, y_I, z_I\}$ represent a right-hand inertia frame with z_I being the vertical direction toward the sky. The body-fixed frame, which is denoted by $\mathcal{B} = \{x_B, y_B, z_B\}$, is located at the center of gravity of the aircraft. The Euclidean position and Euler angle of the UAV with respect to the frame $\{\mathcal{I}\}$ are represented by $\xi(t) = [x(t), y(t), z(t)]^T \in \mathbb{R}^3$ and $\eta(t) = [\phi(t), (t), \psi(t)]^T \in \mathbb{R}^3$.

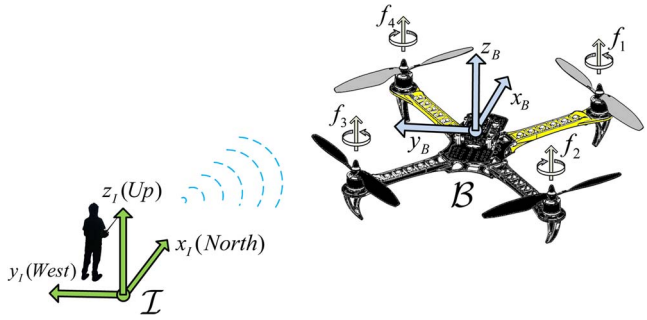

Fig. 1. Schematic of a quadrotor UAV.

The detailed dynamic model of the quadrotor can be found in previous works [21], [22]. In this paper, to implement the control schemes more easily, we apply the assumptions and simplification in [23]. Then, the dynamic model expressed in $\{\mathcal{I}\}$ is given as the following form [18]:

$$\begin{aligned}
m\ddot{x} &= -K_1\dot{x} + (\cos\phi\sin\theta\cos\psi + \sin\phi\sin\psi)u_t \\
m\ddot{y} &= -K_2\dot{y} + (\cos\phi\sin\theta\sin\psi - \sin\phi\cos\psi)u_t \\
m\ddot{z} &= -K_3\dot{z} - mg + (\cos\phi\cos\theta)u_t \\
J_1\ddot{\phi} &= -K_4 l\dot{\phi} + d_1(t) + l\tau_1 \\
J_2\ddot{\theta} &= -K_5 l\dot{\theta} + d_2(t) + l\tau_2 \\
J_3\ddot{\psi} &= -K_6\dot{\psi} + d_3(t) + c\tau_3
\end{aligned} \tag{1}$$

where $m \in \mathbb{R}^+$ denotes the mass, $J_i \in \mathbb{R}^+$ for $i = 1, 2, 3$ are the moments of inertia, $K_i \in \mathbb{R}^+$ for $i = 1, \ldots, 6$ represents the aerodynamic damping coefficient, g is the acceleration of the gravity, $l \in \mathbb{R}^+$ denotes the distance between the epicenter of the UAV and the rotor axis, and $d_i(t) \in \mathbb{R}$ for $i = 1, 2, 3$ represents the unknown time-varying external disturbances. In(1), $u_t(t)$, $\tau_1(t)$, $\tau_2(t)$, and $\tau_3(t)$ denote the total thrust and three rotational forces produced by the four rotors, and $c \in \mathbb{R}^+$ represents a constant force-to-moment factor.

Remark 1: The overall control objective is to design the control input signals to let the quadrotor track time-varying desired trajectories $[x_d(t), y_d(t), z_d(t), \psi_d(t)]^T$.

Remark 2: The system parameters J_i (for $i = 1, 2, 3$), $K_j (j = 1, \ldots, 6)$, l, and c are some unknown positive constants.

The relationship between the control input signals $[u_t, \tau_1, \tau_2, \tau_3]^T$ and the rotor thrusts $[f_1, f_2, f_3, f_4]^T$ is given by

$$\begin{aligned}
u_t &= f_1 + f_2 + f_3 + f_4 \qquad & \tau_1 &= -f_1 - f_2 + f_3 + f_4 \\
\tau_2 &= -f_1 + f_2 + f_3 - f_4 & \tau_3 &= -f_1 + f_2 - f_3 + f_4.
\end{aligned} \tag{2}$$

The rotation speed of each motor ω_i for $i = 1, 2, 3, 4$ can becalculated based on the value of the lifting force f_i.

To simplify the mathematical expression, the dynamic model in (1) can be reorganized in the following form:

$$\begin{aligned}
m\ddot{\xi} + K_\xi\dot{\xi} + mge_3 &= u_t R_{\mathcal{B}}^{\mathcal{I}} \mathrm{R}e_3 \\
J\ddot{\eta} + K_\eta\dot{\eta} - d &= \tau
\end{aligned} \tag{3}$$

where $K_\xi = \text{diag}\{K_1, K_2, K_3\} \in \mathbb{R}^{3\times3}$, $e_3 = [0,0,1]^T \in \mathbb{R}^3$, $J = \text{diag}\{J_1/l, J_2/l, J_3/c\} \in \mathbb{R}^{3\times3}$, $K_\eta = \text{diag}\{K_4, K_5, K_6/c\} \in \mathbb{R}^{3\times3}$, $\tau = [\tau_1, \tau_2, \tau_3]^T \in \mathbb{R}^3$, $d = [(d_1(t)/l), (d_2(t)/l), (d_3(t)/c)]^T \in \mathbb{R}^3$, ${}^{\mathcal{I}}_{\mathcal{B}}R(\eta) \in SO(3)$ denotes the rotation matrix between the body-fixed frame $\{\mathcal{B}\}$ and the inertial frame $\{\mathcal{I}\}$.

Assumption 1: The unknown time-varying disturbance $d_i(t)$ is continuous differentiable and bounded up to its second-order time derivative, i.e., $d_i(t) \in \mathcal{C}^2$ for $i = 1, 2, 3$.

Let $\xi_d(t) = [x_d(t), y_d(t), z_d(t)]^T$ and $\eta_d(t) = [\phi_d(t), \theta_d(t), \psi_d(t)]^T$ be the desired position and the desired attitude, respectively. Let the tracking error signals be defined as

$$E = [\xi - \xi_d,\ \dot{\xi} - \dot{\xi}_d]^T, \quad e = [\eta - \eta_d,\ \dot{\eta} - \dot{\eta}_d]^T \tag{4}$$

and the following expression can be obtained:

$$\dot{E} = \Pi_1 E + \Pi_2(\ddot{\xi} - \ddot{\xi}_d) \quad \dot{e} = \Pi_1 e + \Pi_2(\ddot{\eta} - \ddot{\eta}_d) \tag{5}$$

where $\Pi_1 \in \mathbb{R}^{6\times6}$ and $\Pi_2 \in \mathbb{R}^{6\times3}$ are defined as follows:

$$\Pi_1 = \begin{bmatrix} O_3 & I_3 \\ O_3 & O_3 \end{bmatrix} \quad \Pi_2 = \begin{bmatrix} O^{3\times3} \vdots I_3 \end{bmatrix}^T \tag{6}$$

with $I_3 \in \mathbb{R}^{3\times3}$ denoting a 3×3 identity matrix, and $O_3 \in \mathbb{R}^{3\times3}$ being a 3×3 zero matrix.

The dynamics described in (3) can be considered as a cascaded structure in which the position subsystem (outer loop) and the attitude subsystem (inner loop) are coupled through the rotation matrix ${}^{\mathcal{I}}_{\mathcal{B}}R(\eta)$. Hence, to formulate the problem as the control of two connected systems, a virtual control vector $v = [v_1, v_2, v_3]^T \in \mathbb{R}^3$ is introduced. Then, the open-loop system can be obtained after introducing v and substituting (3) into (5), i.e.,

$$\dot{E} = \underbrace{\Pi_1 E + \Pi_2\left(v - \ddot{\xi}_d - \frac{K_\xi}{m}\dot{\xi}\right)}_{f_E(E,v,\dot{\xi},\ddot{\xi}_d)} + \underbrace{\Pi_2\left(\frac{u_t}{m}Re_3 - ge_3 - v\right)}_{f_\Delta(u_t,v,e)}$$

$$\dot{e} = \underbrace{\Pi_1 e + \Pi_2\left[J^{-1}(\tau - K_\eta\dot{\eta} + d) - \ddot{\eta}_d\right]}_{f_e(e,\tau,\dot{\eta},\ddot{\eta}_d)} \tag{7}$$

where f_Δ is the coupling term that connects the inner- and outer-loop subsystems.

Due to the underactuated property of the quadrotor, it is very difficult to control all the six outputs independently. In this paper, the states to be controlled are selected as $\xi(t)$ and $\psi(t)$; thus, only ξ_d and ψ_d are selected to construct by the guidance system, whereas ϕ_d and θ_d are generated by the solutions of v. Motivated by the work in [22], the virtual control input v can be chosen as the following form:

$$\begin{aligned} v_1 &= \frac{u_t}{m}(\cos\phi_d \sin\theta_d \cos\psi_d + \sin\phi_d \sin\psi_d) \\ v_2 &= \frac{u_t}{m}(\cos\phi_d \sin\theta_d \sin\psi_d - \sin\phi_d \cos\psi_d) \\ v_3 &= \frac{u_t}{m}(\cos\phi_d \cos\theta_d) - g. \end{aligned} \tag{8}$$

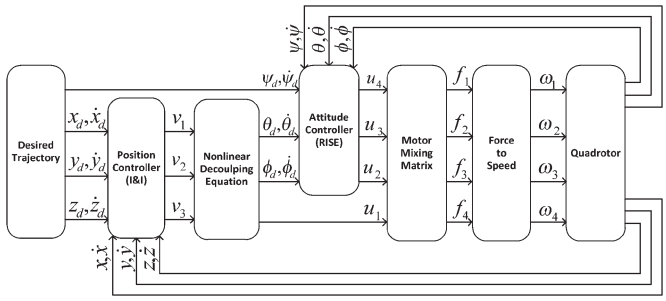

Fig. 2. Structure of the overall control system.

The total thrust u_t and desired angles ϕ_d and θ_d can be solved as

$$\begin{aligned} u_t &= m\sqrt{v_1^2 + v_2^2 + (v_3 + g)^2} \\ \phi_d &= \sin^{-1}\left(\frac{m}{u_t}(v_1 \sin\psi_d - v_2 \cos\psi_d)\right) \\ \theta_d &= \tan^{-1}\left(\frac{1}{v_3 + g}(v_1 \cos\psi_d + v_2 \sin\psi_d)\right). \end{aligned} \tag{9}$$

The control objective is thus to design the control laws $v(E, \ddot{\xi}_d)$ and $\tau(e, \ddot{\eta}_d)$ such that the tracking errors E and e converge to zero asymptotically.

Based on (7), the outer-loop subsystem can be chosen as $\dot{E} = f_E$ in which the coupling term f_Δ is temporarily not considered, and the inner-loop subsystem can be chosen as $\dot{e} = f_e$. Then, the main control development can be achieved in the following three steps:

Step 1: Develop an adaptive control scheme $v = \mu_E(E, \ddot{\xi}_d)$ for the outer-loop subsystem $\dot{E} = f_E$ to ensure that the tracking error E converges to 0 asymptotically.

Step 2: Develop a robust control law $\tau = \mu_e(e, \ddot{\eta}_d)$ for the inner-loop subsystem $\dot{e} = f_e$ to ensure that the tracking error e converges to 0 asymptotically.

Step 3: Considering the closed-loop system where the coupling term $f_\Delta(u_t, v, e)$ is included, prove that the tracking errors E and e converge to 0 asymptotically.

Remark 3: In order to avoid the sudden change of the quadrotor's dynamic states, the reference trajectories $\xi_d^{(i)}$, $\psi_d^{(j)}$ are designed such that $\xi_d^{(i)}, \psi_d^{(j)} \in L_\infty$ for $i = 0, 1, \ldots, 6$ and $j = 0, 1, \ldots, 4$, where (i) represents the ith-order time derivative of the variable.

III. Control Development

This section presents the control design of the inner loop and the outer loop, respectively. To address the parametric uncertainties, an I&I-based adaptive strategy is applied for the controller of the outer loop, while to compensate for the unknown disturbances, the RISE-based scheme is utilized for the controller of the inner loop. The block diagram of the overall control system is shown in Fig. 2.

A. Outer-Loop Controller Design Based on I&I Adaptive Scheme

The objective of this section is to design the auxiliary control input $v(t)$ for the outer-loop subsystem to ensure that the tracking error E converges to zero asymptotically. It is easy to check that the outer-loop subsystem $\dot{E} = f_E$ is equivalent to the following dynamic system:

$$\ddot{\xi} = -\frac{1}{m}K_\xi \dot{\xi} + v. \tag{10}$$

Since K_ξ is uncertain to the control development, an I&I-based adaptive controller is introduced as follows.

Let the position error, which is denoted by $\chi_1 = [\chi_{11}, \chi_{12}, \chi_{13}] \in \mathbb{R}^3$, and its filtered tracking error $\chi_2 = [\chi_{21}, \chi_{22}, \chi_{23}] \in \mathbb{R}^3$ be defined as follows:

$$\chi_1 = \xi - \xi_d \qquad \chi_2 = \dot{\chi}_1 + \alpha\chi_1 \tag{11}$$

where $\alpha = \mathrm{diag}\{\alpha_1, \alpha_2, \alpha_3\} \in \mathbb{R}_+^{3\times 3}$ denotes a diagonal positive-definite gain matrix. After substituting (11) into (10), it can be obtained that

$$\dot{\chi}_1 = -\alpha\chi_1 + \chi_2 \qquad \dot{\chi}_2 = v + \varphi(\chi)s + \rho(\chi) \tag{12}$$

where $\chi = [\chi_1^T, \chi_2^T]^T \in \mathbb{R}^6$, $\varphi(\chi) = -(1/m)\mathrm{diag}\{\dot{\xi}\} \in \mathbb{R}^{3\times 3}$, $\rho(\chi) = \alpha\dot{\chi}_1 - \ddot{\xi}_d \in \mathbb{R}^3$, and $s = K_\xi \in \mathbb{R}^3$. It is not difficult to check that $\varphi(\cdot)$ and $\rho(\cdot)$ are smooth function matrices and do not contain any unknown system parameters.

Let the estimation error $\zeta = [\zeta_1, \zeta_2, \zeta_3]^T \in \mathbb{R}^3$ be defined as

$$\zeta = \hat{s} - s + \beta(\chi) \tag{13}$$

where $\hat{s} = [\hat{s}_1, \hat{s}_2, \hat{s}_3]^T \in \mathbb{R}^3$ is the online estimation for the unknown system parameter vector s, and $\beta(\chi) = [\beta_1(\chi), \beta_2(\chi), \beta_3(\chi)]^T \in \mathbb{R}^3$ is a continuous function vector that will be designed later. After differentiating (13) with respect to time, the dynamics of ζ is given by

$$\dot{\zeta} = \dot{\hat{s}} + \frac{\partial\beta}{\partial\chi_1^T}\dot{\chi}_1 + \frac{\partial\beta}{\partial\chi_2^T}\left(v + \varphi\cdot(\hat{s} + \beta - \zeta) + \rho\right). \tag{14}$$

Based on (14) and the following stability analysis, the adaptive state feedback update law $\dot{\hat{s}}$ and virtual control input v are designed as follows:

$$\dot{\hat{s}} = -\frac{\partial\beta}{\partial\chi_1^T}\dot{\chi}_1 - \frac{\partial\beta}{\partial\chi_2^T}\left(v + \varphi\cdot(\hat{s} + \beta) + \rho\right) \tag{15}$$

$$v = -k_\chi\chi_2 - \varepsilon\chi_1 - \varphi\cdot(\hat{s} + \beta) - \rho \tag{16}$$

$$\beta_i = \gamma_i \int_0^{\chi_{2i}} \varphi_i(\chi_1, \sigma)d\sigma, \quad \text{for} \quad i = 1, 2, 3 \tag{17}$$

where $k_\chi = \mathrm{diag}\{k_{\chi1}, k_{\chi2}, k_{\chi3}\} \in \mathbb{R}_+^{3\times 3}$, $\varepsilon = \mathrm{diag}\{\varepsilon_1, \varepsilon_2, \varepsilon_3\} \in \mathbb{R}_+^{3\times 3}$, and $\gamma = \mathrm{diag}\{\gamma_1, \gamma_2, \gamma_3\} \in \mathbb{R}_+^{3\times 3}$ are some diagonal positive-definite gain matrices, and φ_i represents the ith element on the principal diagonal of matrix φ.

By substituting (15)–(17) into (14), the following dynamics of $\dot{\zeta}$ can be obtained:

$$\dot{\zeta} = -\gamma\cdot\varphi^2(\chi)\cdot\zeta. \tag{18}$$

By substituting (13) and (16) into (12), the closed-loop dynamics of χ_1 and χ_2 can be formulated as

$$\dot{\chi}_1 = -\alpha\chi_1 + \chi_2 \tag{19}$$

$$\dot{\chi}_2 = -k_\chi\chi_2 - \varepsilon\chi_1 - \varphi(\chi)\cdot\zeta. \tag{20}$$

Theorem 1: Given the closed-loop dynamics defined by (19) and (20), the control input given in (16), the adaptation law in (15), along with the auxiliary functions β_i defined in (17) ensures an asymptotically stable (AS) result of the tracking error χ in the sense that

$$\chi \to 0 \quad \text{as} \quad t \to \infty. \tag{21}$$

Proof: Let $V_\zeta(t) \in \mathbb{R}$ denote the following nonnegative function:

$$V_\zeta(t) = \zeta^T\gamma^{-1}\zeta. \tag{22}$$

After taking the time derivative of (22) and substituting (18), the following expression can be obtained:

$$\dot{V}_\zeta(t) = -2\zeta^T\varphi^2(\chi)\zeta = -2\sum_{i=1}^{3}\varphi_i^2\cdot\zeta_i^2 \le 0. \tag{23}$$

From (22) and (23), it can be concluded that $\varphi(\chi)\cdot\zeta(\chi) \in \mathcal{L}_2$. Then, it is obvious that $\zeta(t)$ is stable, and the system in (19) and (20) is an AS system perturbed by an $\mathcal{L}_2$ signal.

Based on the above conclusion, let $W(\chi, \zeta) \in \mathbb{R}$ denote a Lyapunov function candidate, which is defined as follows:

$$W(\chi, \zeta) = \chi_1^T\varepsilon\chi_1 + \chi_2^T\chi_2 + \zeta^T\gamma^{-1}k_\chi^{-1}\zeta. \tag{24}$$

Taking the time derivative of (24) and substituting (18)–(20) into the resulting equation yields

$$\begin{aligned}\dot{W} &= -2\chi_1^T\varepsilon\alpha\chi_1 - 2\chi_2^Tk_\chi\chi_2 - 2\chi_2^T\varphi\zeta - 2\zeta^Tk_\chi^{-1}\varphi^2\zeta \\ &\le -2\chi_1^T\varepsilon\alpha\chi_1 - \chi_2^Tk_\chi\chi_2 - \zeta^Tk_\chi^{-1}\varphi^2\zeta \\ &= \sum_{i=1}^{3}\left(-2\varepsilon_i\alpha_i\chi_{1i}^2 - k_{\chi i}\chi_{2i}^2 - k_{\chi i}^{-1}(\varphi_i\zeta_i)^2\right) \le 0.\end{aligned} \tag{25}$$

The results in (25) implies that the estimation error system (18) has a stable equilibrium at the origin; thus, the closed-loop system (19) and (20) has a stable equilibrium at $(0, s)$. It can be also concluded that all the trajectories converge to the following invariant set:

$$\mathcal{M} = \{(\chi, \zeta) : \chi = 0, \varphi(\chi)\cdot\zeta = 0\}. \tag{26}$$

Then, LaSalle's invariance theorem can be used to prove the result in (21). ■

Remark 4: By substituting (16) into (9) and utilizing Remark 2, it is not difficult to show that $\phi_d^{(i)}, \theta_d^{(j)} \in \mathcal{L}_\infty$ for $i, j = 0, 1, \ldots, 4$. This conclusion will be invoked later.

Remark 5: The estimation $\hat{s}(t)$ can be used for compensating the parametric uncertainties and maintaining the stability of the system. However, there is no guarantee that $\hat{s}(t)$ finally converges to the true value of s because the dynamic system in (10) does not meet the persistent-excitation condition [12].

Remark 6: When implementing the proposed control design in practice, expressions (15)–(17) can be rewritten as

$$\dot{\hat{s}} = -\gamma\varphi\left[v + \varphi\cdot\left(\hat{s} - \frac{1}{m}\dot{\xi}\gamma\chi_2\right) + \rho\right] \tag{27}$$

$$v = -k_\chi\chi_2 - \varepsilon\chi_1 - \varphi\cdot\left(\hat{s} - \frac{1}{m}\dot{\xi}\gamma\chi_2\right) - \rho \tag{28}$$

$$\beta = -\frac{1}{m}\dot{\xi}\gamma\chi_2. \tag{29}$$

B. Inner-Loop Controller Design Based on RISE Method

The objective of this section is to design a proper inner-loop control scheme τ, which will ensure the asymptotic convergence of the tracking error $e(t)$ in (7).

Before presenting the RISE control law, some auxiliary error signals shall be defined first. The attitude tracking error, which is denoted by $r_1 \in \mathbb{R}^3$, and its filtered error signals $r_2, r_3 \in \mathbb{R}^3$ are defined as follows:

$$r_1 = \eta - \eta_d \quad r_2 = \dot{r}_1 + \lambda r_1 \quad r_3 = \dot{r}_2 + \Lambda r_2 \tag{30}$$

where $\lambda = \mathrm{diag}\{\lambda_1, \lambda_2, \lambda_3\} \in \mathbb{R}_+^{3\times3}$ and $\Lambda = \mathrm{diag}\{\Lambda_1, \Lambda_2, \Lambda_3\} \in \mathbb{R}_+^{3\times3}$ are some diagonal positive-definite gain matrices.

The open-loop dynamic system of the tracking error signal r_3 can be obtained by taking the time derivative of the third entry of (30), multiplying the resulting equation by J and substituting (3) into the resulting equation as follows:

$$J\dot{r}_3 = -K_\eta\ddot{\eta} + \dot{d} + \dot{\tau} - J\dddot{\eta}_d + J\lambda\ddot{r}_1 + J\Lambda\dot{r}_2. \tag{31}$$

Let the auxiliary functions $N(\eta^{(i)}, t)$, $N_d(t)$, and $\tilde{N}(t)$ be defined as

$$\begin{aligned} N\left(\eta^{(i)}, t\right) &= -K_\eta\ddot{\eta} + \dot{d} - J\dddot{\eta}_d + J\lambda\ddot{r}_1 + J\Lambda\dot{r}_2 + r_2 \\ N_d(t) &= N\left(\eta_d^{(i)}, t\right) = -K_\eta\ddot{\eta}_d + \dot{d} - J\dddot{\eta}_d \\ \tilde{N} &= N - N_d = -K_\eta\ddot{r}_1 + J\lambda\ddot{r}_1 + J\Lambda\dot{r}_2 + r_2 \end{aligned} \tag{32}$$

then (31) can be rewritten as

$$J\dot{r}_3 = -r_2 + \dot{\tau} + N_d + \tilde{N}. \tag{33}$$

Due to Remark 4, it can be checked that $N_d(t), \dot{N}_d(t) \in \mathcal{L}_\infty$, and $N(\cdot)$ are continuously differentiable. It is easy to show that $\tilde{N}$ can be upper bounded as follows:

$$\|\tilde{N}\| \le \varrho\cdot\|r\| \tag{34}$$

where $\|\cdot\|$ denotes the Euclidean norm, $r(t) \in \mathbb{R}^9$ is defined as $r := [r_1^T, r_2^T, r_3^T]^T$, and ϱ is some positive constant.

Similar to the control development in [19] and [20], the following robust attitude controller is proposed:

$$\dot{\tau} = -(k_r + I_3)r_3 - 2\Gamma sgn(r_2) \tag{35}$$

where $k_r = \mathrm{diag}\{k_{r1}, k_{r2}, k_{r3}\} \in \mathbb{R}_+^{3\times3}$ and $\Gamma = \mathrm{diag}\{\Gamma_1, \Gamma_2, \Gamma_3\} \in \mathbb{R}_+^{3\times3}$ are some diagonal positive-definite control gain matrices, and I_3 is a 3×3 identity matrix. By substituting (35) into (33), the following closed-loop system of r_3 can be obtained:

$$J\dot{r}_3 = -(k_r + I)r_3 - 2\Gamma sgn(r_2) - r_2 + N_d + \tilde{N}. \tag{36}$$

Remark 7: By using the knowledge of *Filippov Solution* in Appendix A, it can be concluded that r_3 is absolutely continuous and satisfies

$$J\dot{r}_3 \in -(k_r + I)r_3 - 2\Gamma SGN_k(r_2) - r_2 + N_d + \tilde{N} \tag{37}$$

where $SGN_k(\cdot)$ is a set-value function such that

$$SGN_k(x) = \begin{cases} -1 & , \quad x < 0 \\ [-1, 1], & x = 0 \\ 1 & , \quad x > 0. \end{cases} \tag{38}$$

Theorem 2: Given the error system defined by (31) and under the following sufficient conditions:

$$\Gamma_i \ge \|N_{di}\|_\infty + \Lambda_i^{-1}\|\dot{N}_{di}\|_\infty, \quad \text{for} \quad i = 1, 2, 3 \tag{39}$$

the control input given in (35) ensures a locally exponentially stable (LES) result of the tracking error r; in other words, there exist two positive constants α_η, γ_η such that

$$\forall\, t > 0, \|r(t)\| \le \alpha_\eta\cdot\exp(-\gamma_\eta t). \tag{40}$$

Proof: Before introducing the Lyapunov candidate function, let the auxiliary functions $Q_\eta(t) \in \mathbb{R}$ be defined as

$$Q_\eta(t) = \int_0^t 2\dot{r}_2^T\Gamma\,\mathrm{sgn}(r_2)d\sigma + 2\sum_{i=1}^3\Gamma_i\,|r_{2i}(0)| - N_d^T r_2. \tag{41}$$

By utilizing the sufficient condition of Γ_i in (39), the following inequality holds:

$$\begin{aligned} Q_\eta(t) &= 2\sum_{i=1}^3\Gamma_i\,|r_{2i}(t)|_0^t + 2\sum_{i=1}^3\Gamma_i|r_{2i}(0)| - N_d^T r_2 \\ &\ge 2\sum_{i=1}^3\left(\frac{\|N_{di}\|_\infty}{2} + \Lambda_i^{-1}\|\dot{N}_{di}\|_\infty\right)|r_{2i}| \ge 0. \end{aligned} \tag{42}$$

Let $V_\eta(r, t) \in \mathbb{R}$ denote the following nonnegative function:

$$V_\eta = \frac{1}{2}r_1^T r_1 + \frac{1}{2}r_2^T r_2 + \frac{1}{2}r_3^T J r_3 + Q_\eta(t). \tag{43}$$

The function V_η can be upper and lower bounded as

$$V_\eta \ge J^*\|r\|^2 \tag{44}$$

$$V_\eta \le J^+\|r\|^2 + \sum_{i=1}^3\left(2\Gamma_i + \|N_{di}\|_\infty\right)|r_{2i}(t)| \tag{45}$$

where $J^* = (1/2)\min\{1, J_i\}$, and $J^+ = (1/2)\max\{1, J_i\}$ for $i = 1, 2, 3$.

Before differentiating $V_\eta(t)$, let the generalized gradient $\partial V(t) \in \mathbb{R}^{12}$ be defined as

$$\partial V(t) = \left[r_1^T, r_2^T + 2SGN_v\left(r_2^T\right)\Gamma - N_d^T, r_3^T, -r_2^T\dot{N}_d\right] \tag{46}$$

where $SGN_v(\cdot)$ is *Clarke's generalized gradient* of $|\cdot|$. By utilizing the *chain rule* in [24], it can be obtained that

$$\dot{V}_\eta(t) \overset{a.e.}{\in} \dot{\tilde{V}}_\eta \equiv \bigcap_{V_d\in\partial V} V_d\begin{bmatrix} K_s(r) \\ 1^{3\times1}\end{bmatrix} \tag{47}$$

where

$$K_s(r) = \begin{bmatrix} r_2 - \lambda r_1 \\ r_3 - \Lambda r_2 \\ -(k_r + I)r_3 - 2\Gamma SGN_k(r_2) - r_2 + N \end{bmatrix} \tag{48}$$

and it is not difficult to show that

$$\left[\dot{r}_1^T,\ \dot{r}_2^T,\ \dot{r}_3^T\right]^T \overset{a.e.}{\in} K_s(r). \tag{49}$$

Remark 8: Details about the definition of *Clarke's generalized gradient* and the lemma of *chain rule* can be found in Appendix A.

For all $s_v \in SGN_v(r_2)$, $s_k \in SGN_k(r_2)$, $\dot{\tilde{V}}_\eta(t)$ can be deduced as

$$\begin{aligned} \dot{\tilde{V}}_\eta = \bigcap_{s_v \in SGN_v(r_2)} \Big\{ & -r_1^T \lambda r_1 + r_1^T r_2 - r_2^T \Lambda r_2 + r_3^T \tilde{N} \\ & - r_3^T (k_r + I) r_3 - 2 r_2^T \Gamma \Lambda s_k - r_2^T \dot{N}_d \\ & + r_2^T \Lambda N_d + 2 \dot{r}_2^T \Gamma (s_v - s_k) \Big\}. \end{aligned} \tag{50}$$

In the case that $r_2 \neq 0$, it can be obtained that $s_v - s_k = 0$, and in the case that $r_2 = 0$, the following equations hold:

$$\begin{aligned} \bigcap_{s_v \in SGN_v(r_2)} \{s_v - s_k\} &= \bigcap_{s_v \in [-1,1]} \{s_v - [-1,1]\} \\ &= \bigcap_{s_v \in [-1,1]} \{[s_v - 1, s_v + 1]\} = 0. \end{aligned}$$

Thus, it can be obtained that

$$\begin{aligned} \dot{\tilde{V}}_\eta = & -r_1^T \lambda r_1 + r_1^T r_2 - r_2^T \Lambda r_2 + r_3^T \tilde{N} \\ & - r_3^T (k_r + I) r_3 - \sum_{i=1}^{3} \Gamma_i \Lambda_i |r_{2i}| + O_\eta(t) \end{aligned} \tag{51}$$

where $O_\eta(t) = -\sum_{i=1}^{3} \Gamma_i \Lambda_i |r_{2i}| - r_2^T \dot{N}_d + r_2^T \Lambda N_d$. By applying the sufficient condition in (39), the following inequality holds:

$$O_\eta(t) \leq \sum_{i=1}^{3} \left(-\Gamma_i \Lambda i + \Lambda_i \|N_{di}\|_\infty + \|\dot{N}_{di}\|_\infty \right) |r_{2i}| \leq 0.$$

The utilization of (34) and (39) yields the following inequality for $\dot{\tilde{V}}_\eta$:

$$\begin{aligned} \dot{\tilde{V}}_\eta &\leq -2\lambda^* \|r\|^2 - k^* \|r_3\|^2 + r_3^T \tilde{N} - \sum_{i=1}^{3} \Gamma_i \Lambda_i |r_{2i}| \\ &\leq -\lambda^* \|r\|^2 - \left(\lambda^* - \frac{\varrho^2}{4k^*} \right) \|r\|^2 - \sum_{i=1}^{3} \Gamma_i \Lambda_i |r_{2i}| \end{aligned} \tag{52}$$

where $\lambda^* = (1/2) \min_{i=1,2,3} \{\lambda_i - (1/2), 1\} \in \mathbb{R}^+$, $k^* = \min\{k_r\} \in \mathbb{R}^+$. If the following sufficient condition is satisfied:

$$k^* \geq \frac{\varrho^2}{4\lambda^*} \tag{53}$$

then the inequality in (52) can be rewritten as

$$\dot{\tilde{V}}_\eta \leq -\sum_{i=1}^{3} \Gamma_i \Lambda_i |r_{2i}| - \lambda^* \|r\|^2. \tag{54}$$

The bounded properties in (45) and (54) can be used to determine that there exists a positive constant $C_\eta \in \mathbb{R}^+$ satisfying

$$\dot{\tilde{V}}_\eta(t) \leq -C_\eta \cdot V_\eta(t) \tag{55}$$

where C_η can be chosen as

$$0 < C_\eta \leq \min_{i=1,2,3} \left\{ \frac{\lambda^*}{J^+}, \frac{\Gamma_i \Lambda_i}{2\Gamma_i + \|N_{di}\|_\infty} \right\}. \tag{56}$$

Since $\dot{V}_\eta \in \dot{\tilde{V}}_\eta$, then it can be also concluded that $\dot{V}_\eta(t) \leq -C_\eta \cdot V_\eta(t)$, which implies that

$$V_\eta(t) \leq V_\eta(0) \exp(-C_\eta t). \tag{57}$$

By using the bounded properties in (44), it can be further obtained that

$$\|r\| \leq \sqrt{\frac{V_\eta(0)}{J^*}} e^{-\frac{C_\eta}{2} t}. \tag{58}$$

Then, the LES of the tracking error r is proved. ■

Remark 9: Based on the definition of E, e, χ, and r, (21) and (40) can be utilized to conclude the AS result of the tracking error E and the LES result of the tracking error e.

IV. Stability Analysis

It is necessary to point out that, due to the existence of the coupling term f_Δ in (7), Theorems 1 and 2 cannot be used to determine the stability of the closed-loop system directly. Hence, the following lemma is invoked to analyze the stability of the cascaded systems.

Lemma 1: There is a feedback v such that E is an AS equilibrium of the system $\dot{E} = f_E(E, v, \ddot{\xi}_d)$, then any partial state feedback control τ that renders the equilibrium of $\dot{e} = f_e(e, \tau, \ddot{\eta}_d)$ subsystem $e = 0$ also achieves AS of $(E, e) = (0, 0)$.

Proof: See the proof in [25]. ■

The AS of the connected system (7) can be determined if all the trajectories in $(E(t), e(t))$ are bounded. In order to prove the boundedness of the system trajectories, the following lemma is introduced.

Lemma 2: Let τ be some $\mathcal{C}^1$ partial state feedback such that the equilibrium point $e = 0$ is LES. Suppose that there exist a $c_1 \in \mathbb{R}^+$ and a class-$\mathcal{K}$ function $\kappa(\cdot)$ that is differentiable at $e = 0$ such that

$$\|E\| \geq c_1 \Longrightarrow \|f_\Delta(E, r_1)\| \leq \kappa(\|r_1\|) \|E\|. \tag{59}$$

If there exists a positive semidefinite radially unbounded function $V_s(E)$ and $c_2, c_3 \in \mathbb{R}^+$ such that for $\|E\| \geq c_2$

$$\frac{\partial V_s}{\partial E} f(E, v, \ddot{\xi}_d) \leq 0 \tag{60}$$

$$\left\| \frac{\partial V_s}{\partial E} \right\| \|E\| \leq c_3 V_s(E) \tag{61}$$

the feedback τ guarantees the boundedness of all the solutions of (7).

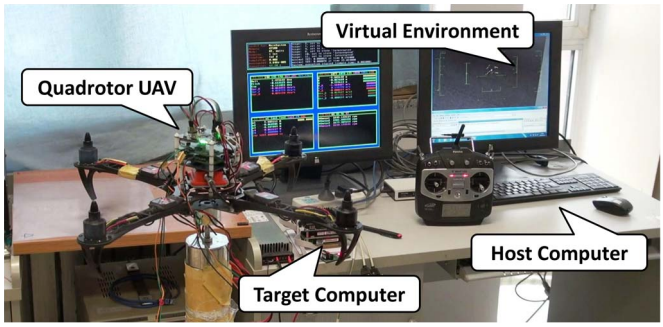

Fig. 3. Quadrotor UAV HILS testbed.

Proof: See the proof in [10]. ■

Therefore, the problem is reduced to ensuring that the closed-loop system controlled by v and τ satisfies (59)–(61) in the lemmas above, and the following lemmas will finish this proof.

Lemma 3: There exist some positive constants r_t and k_t such that $u_t(E)$ satisfies the following properties:

$$|u_t(E)| \leq \begin{cases} k_t\|E\|, & \text{for } \|E\| \geq r_t \\ k_t r_t, & \text{for } \|E\| < r_t. \end{cases} \tag{62}$$

Lemma 4: There exists a positive constant k_H such that $H(E, r_1)$ satisfies the following inequality:

$$\|H(E, r_1)\| \leq k_H \|r_1\|. \tag{63}$$

Lemma 5: Considering the dynamic system $\dot{E} = f_E$, the conditions described in (60) and (61) hold.

The proofs of Lemmas 3–5 are given in Appendix B.

Theorem 3: Given the control design in (16) and (35) and the adaptive update law in (15) and (17), the closed-loop system (7) has an AS equilibrium at $(E, e) = (0, 0)$.

Proof: From Theorems 1 and 2 and Lemmas 1–5, the AS of the equilibrium point $(E, e) = (0, 0)$ is guaranteed.

V. Experimental Results

A. Testbed

To implement the control laws presented in Section III and verify the control performance, an xPC Target-based HILS testbed is employed. A snapshot of the complete HILS environment is shown in Fig. 3, and the testbed consists of the following components.

1) *Miniature quadrotor helicopter*: The quadrotor is a typical X450 commercial helicopter. In order to implement the proposed algorithms, a self-made digital signal processor board is utilized as the main on-board MCU. To estimate the attitude states and the angular velocities, an MTi attitude heading reference system unit from Xsens Inc. is employed as the onboard sensor.
2) *Self-made ball joint*: The quadrotor is fixed on the joint ball, which gives the helicopter free yaw motion and $\pm 40^\circ$ motion range for the pitch and roll rotation. In order to guarantee unrestrained rotational dynamics, the ball joint is located at the central axis of the aircraft.
3) *Simulation computers*: The HILS environment is based on xPC Target, which uses a desktop PC as the host computer and a compact PC/104 computer board as the target computer. The host computer is used to build the simulation model via MATLAB/Simlink, whereas the target computer executes the real-time control commands. A nonlinear dynamic mode of the quadrotor's translational motion is running on the host computer. This dynamic model can receive the actual feedback of the quadrotor's attitude states and then calculate the quadrotor's translational motion with high fidelity. The HILS system is running at a high sampling frequency of 500 Hz.
4) *Virtual simulator clients*: A virtual environment based on FlightGear and Google Earth is developed to display the flight states and flight path, which are calculated by the host computer.

B. Experiment Results and Discussion

To validate the tracking performance and the robustness of the proposed scheme, three cases of experiments are implemented on the HILS testbed. Videos of the HILS experiments are available at the following website.

Case 1: http://youtu.be/OS9uEj9LyzQ.
Case 2: http://youtu.be/Wmn_GgdzEL4.
Case 3: http://youtu.be/j3Kk6cCCfGM.

The quadrotor's system parameters are listed as: $m = 1$ kg, $g = 9.8$ m/s^2, $K_i = 0.01$ Ns/m for $i = 1, 2, 3$. The control gains are chosen as: $\lambda = \{1.5, 1.5, 2\}$, $\Lambda = \{0.08, 0.08, 0.1\}$, $k_r = \{6, 6, 4\}$, $\Gamma = \{1, 1, 1.5\}$, $\alpha = \{0.75, 0.75, 0.75\}$, $k_\chi = \{0.8, 0.8, 0.6\}$, $\varepsilon = \{0.5, 0.5, 0.5\}$, $\gamma = \{2, 2, 8\}$.

Among the control gains above, $\lambda, \Lambda, \alpha, \varepsilon, k_\chi, k_r$ are actually equivalent to the PD control gains, so the standard tuning experience for the PD controller can be directly employed for them. The adaptation gains γ are gradually increased from 0 to achieve faster adaptation until no significant performance improvement is noticed. Considering the sufficient conditions in (39) and (53), k_r and Γ can be first estimated approximately and then selected sufficiently large. In practice, the final selection of the control gains is partially based on the calculation but mainly depend on the actual flight performance.

Case 1—Trajectory Tracking: The quadrotor is tracking a circle in the X-Y plane. The radius of the trajectory is set as 10 m, and the time period of flying one complete circle is set as 40 s. In order to avoid violent motion, the altitude reference trajectory $z_d(t)$ is designed to softly lift off from the start point, rise up, and stay at 1 m high above the ground. After about 10 s of system initialization, the tracking action is started by switching a specific channel on the remote controller. The experiment lasts for more than 140 s, providing enough time to accomplish the circle for three times. The dynamic states of the quadrotor, including the numerically calculated position, the real attitude feedback, and the tracking error, are shown in Figs. 4–7. The virtual control input signals u_t and τ are shown in Fig. 8. The adaptive parameters are presented in Fig. 9.

In Figs. 4–7, the experimental results show good asymptotic tracking performance of the proposed control strategy. It must be pointed out that the control performance of the outer loop directly benefits from the very fast response of the inner-loop controller. It is obvious that both the position errors and attitude errors are driven within a very small range quickly. From the update laws in (15), it is obvious that the changes of the adaptive

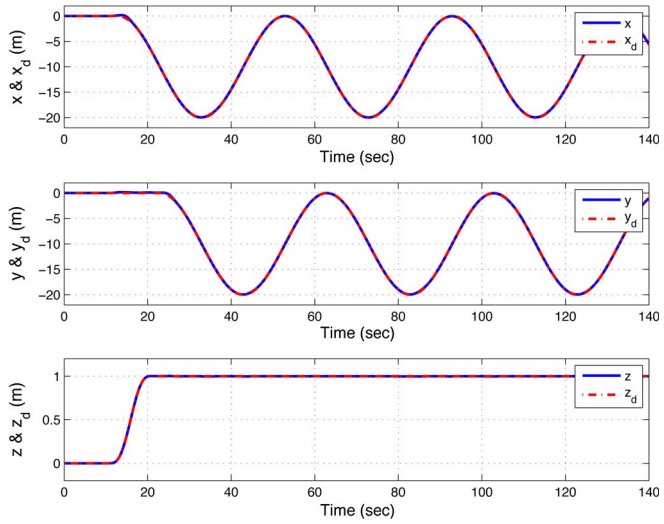

Fig. 4. Desired position (x_d, y_d, z_d) and actual position (x, y, z) in Case 1.

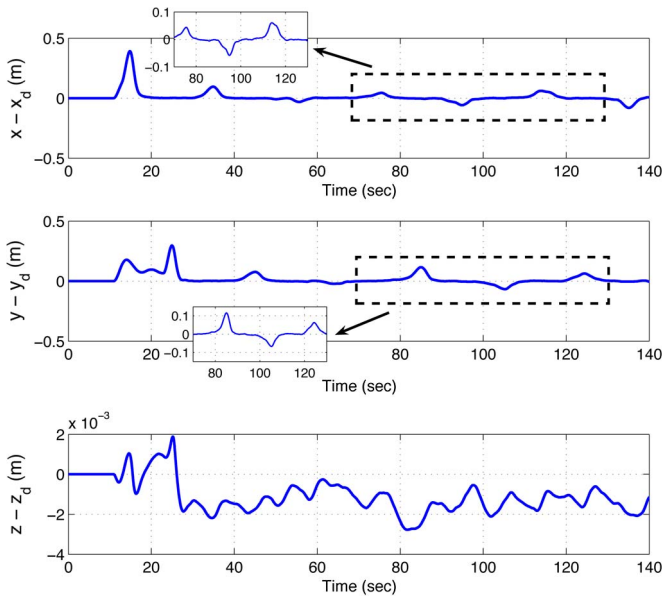

Fig. 5. Position tracking error (e_x, e_y, e_z) in Case 1.

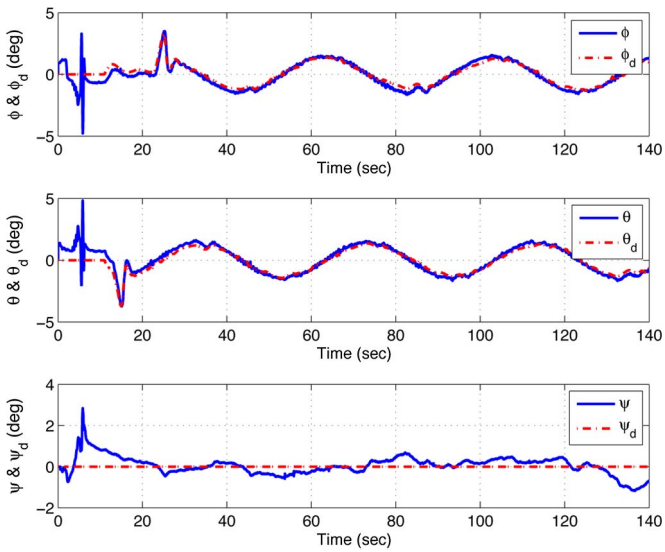

Fig. 6. Desired attitude $(\phi_d, \theta_d, \psi_d)$ and actual attitude (ϕ, θ, ψ) in Case 1.

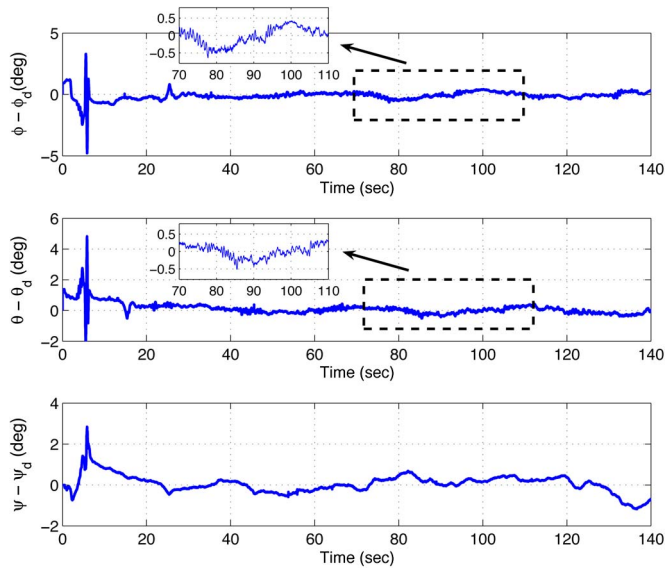

Fig. 7. Attitude tracking error $(e_\phi, e_\theta, e_\psi)$ in Case 1.

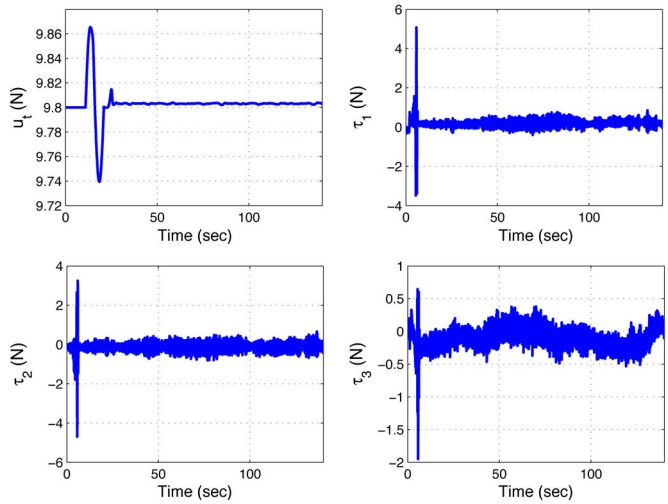

Fig. 8. Total thrust u and rotational forces τ in Case 1.

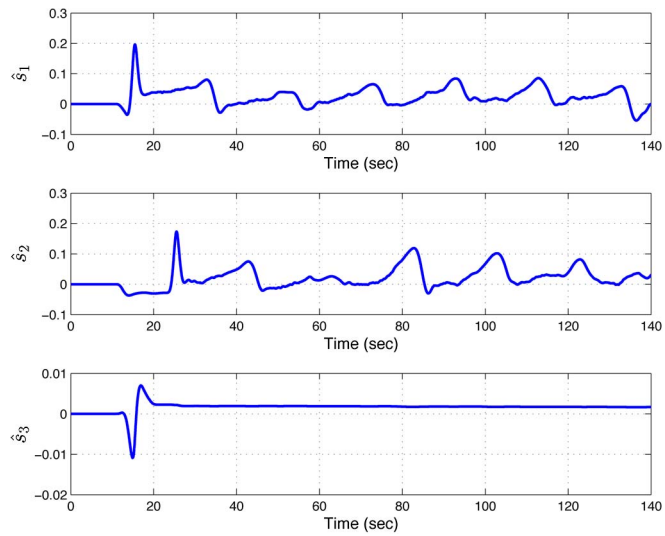

Fig. 9. Adaptive parameters $(\hat{s}_1, \hat{s}_2, \hat{s}_3)$ in Case 1.

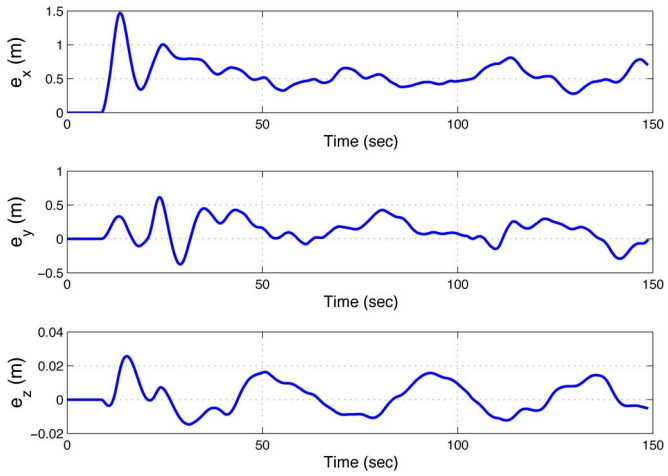

Fig. 10. Position tracking error (e_x, e_y, e_z) in Case 2.

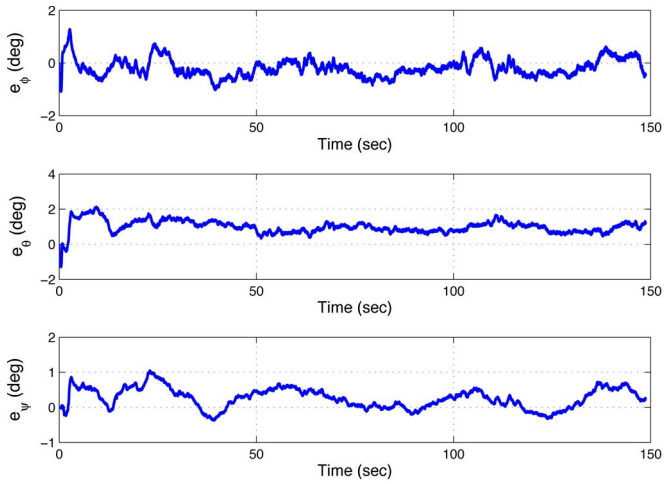

Fig. 11. Attitude tracking error $(e_\phi, e_\theta, e_\psi)$ in Case 2.

estimators are influenced by the tracking errors. In Fig. 9, the estimation values are steadily waving up and down due to the existence of the small tracking error as shown in Fig. 5, and the values are not diverged because the convergence of the adaptive parameters are in accordance with tracking errors.

Case 2—Trajectory Tracking With PD Law: In this case, for comparing and analyzing the effectiveness of the proposed method, a standard PD controller is implemented for the inner- and outer-loop subsystems. The quadrotor is tracking exactly the same trajectory as in Case 1. The tracking errors are shown in Figs. 10 and 11. In Fig. 10, it can be seen that in Case 2, the horizontal-position errors are larger than ± 0.5 m, whereas comparing with Fig. 5 in Case 1, the errors are within ± 0.1 m. In Fig. 11 in Case 2, the attitude tracking errors are larger than $\pm 1.5^\circ$, whereas in Fig. 7, the errors in Case 1 are smaller than $\pm 0.5^\circ$. Thus, it can be seen that the proposed control strategy employed in Case 1 shows a much better performance than the PD control law due to its adaptive and robust properties.

Case 3—Regulation With Disturbances: The control objective in this case is to keep the quadrotor at the point of (0, 0, 1), whereas the initial position of the aircraft is set as $(1.5, -1, 0)$, and $z_d(t)$ is designed in the same way as in *Case 1*. The experiment procedure is similar to *Case 1* except that

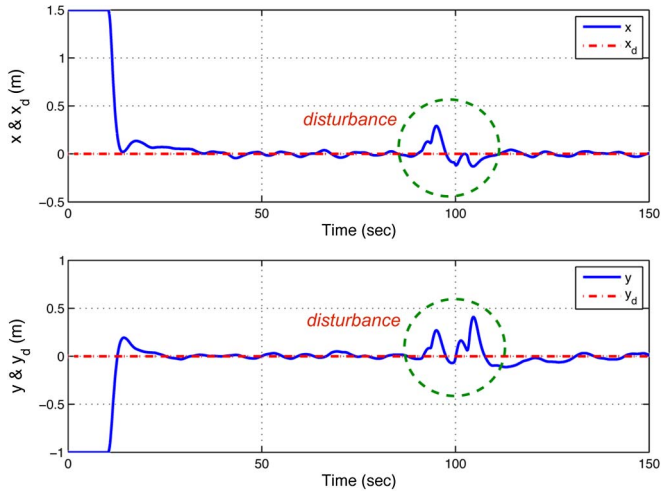

Fig. 12. Actual horizontal position (x, y) and desired horizontal-position trajectories (x_d, y_d) in Case 3.

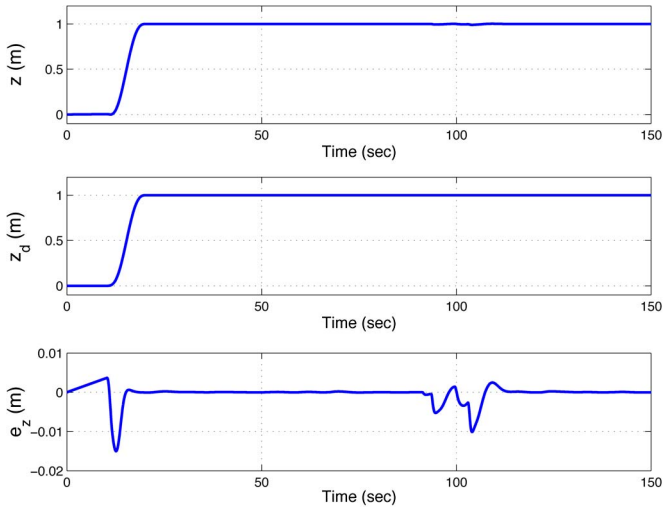

Fig. 13. Actual altitude position z, desired altitude trajectory z_d, and tracking error e_z in Case 3.

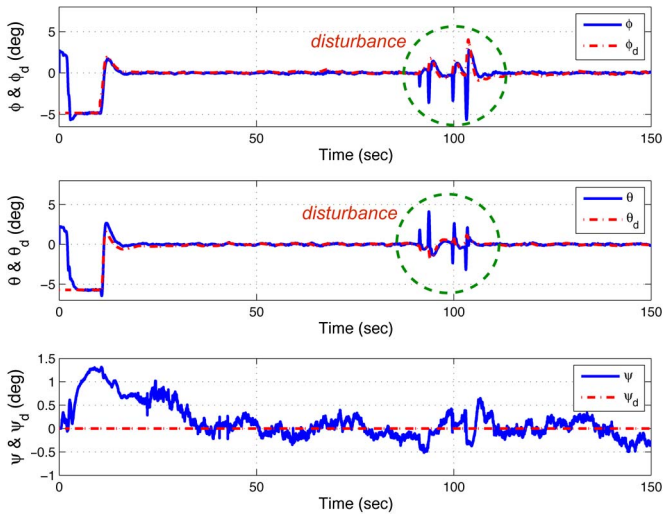

Fig. 14. Desired attitude trajectory $(\phi_d, \theta_d, \psi_d)$ and actual attitude (ϕ, θ, ψ) in Case 3.

during the hovering, the aircraft is disturbed by hand (from 91″ to 106″) to test the robustness of the system. Results of *Case 3* are presented in Figs. 12–17.

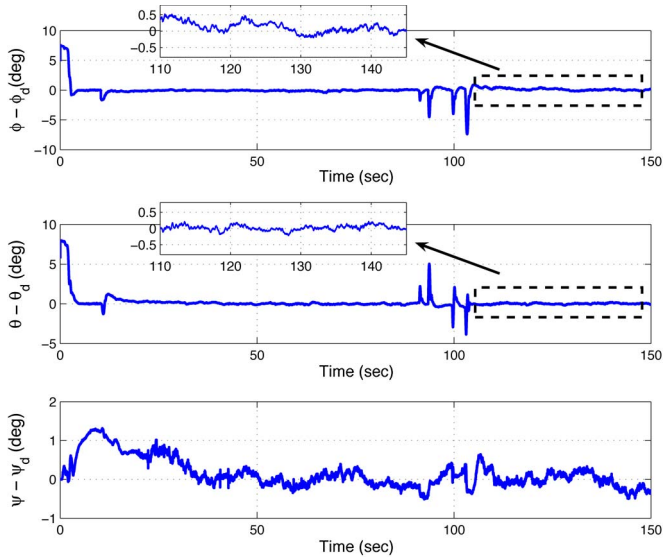

Fig. 15. Attitude tracking error $(e_\phi, e_\theta, e_\psi)$ in Case 3.

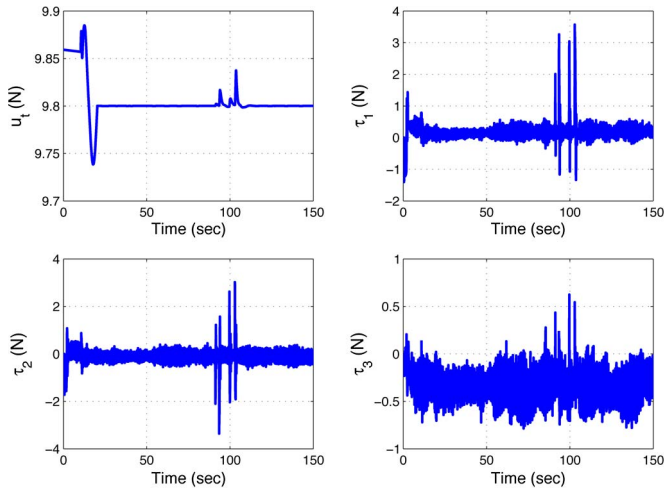

Fig. 16. Total thrust u and rotational forces τ in Case 3.

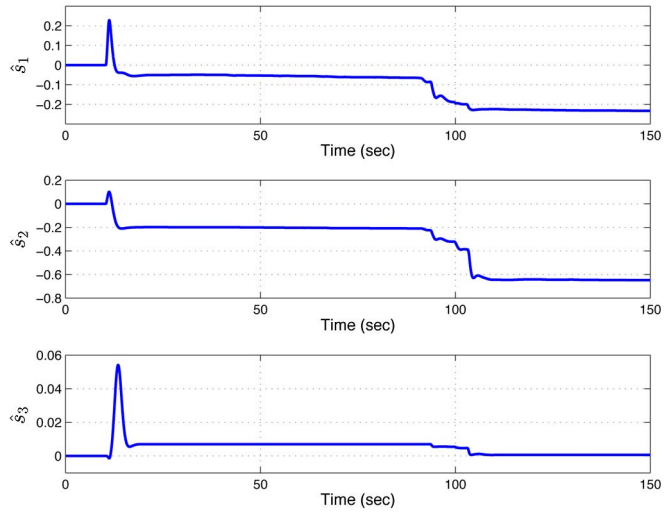

Fig. 17. Adaptive parameters $(\hat{s}_1, \hat{s}_2, \hat{s}_3)$ in Case 3.

In Fig. 12, it can be seen that the proposed control scheme drives the quadrotor to the goal position in a short time (less than 2.5 s) with small overshoot (less than 20%). When reaching the target position, the aircraft is then hovering around it within a very small range (smaller than ± 5 cm). After steadily flying for 60 s, the bottom of motor #2 is bumped up twice by hand to manually break the hovering state. Three seconds later, similar disturbances are introduced on motor #1. These disturbances cause both the shaking of the attitude and the changes of the position. It is clear that the closed-loop system reinstates the previous stable status quickly as soon as the disturbances disappear.

In Fig. 17, before the disturbance being introduced, the tracking errors and the updating signal of $\dot{\hat{s}}(t)$ are almost 0, so the values of the adaptive estimators converge to some constants. The disturbances not only break the hovering status but also increase both the rotational and translational errors. Then, the update laws in (15) are excited to change the value of $\hat{s}(t)$ and further change the control input v. When the system returns to the target position again, $\hat{s}(t)$ stops changing itself. Despite that $\hat{s}(t)$ reaches a different value, the closed-loop system is still kept stable.

Remark 10: It is necessary to highlight that the translational dynamics are calculated based on the actual attitude feedback, which means that the rotation of the quadrotor directly affects the position; meanwhile, the position changes straightly adjust the actual rotation. Hence, although the translational dynamics are simulated by the host computer, the results are still very reliable as reference for the future outdoor flight test.

VI. Conclusion

A nonlinear robust controller for a quadrotor has been presented under the parametric uncertainties and unknown external disturbances, which can achieve asymptotic tracking of the time-varying reference trajectory. The RISE method and the I&I adaptive approach are utilized to formulate the inner-loop and the outer-loop structural control scheme. The Lyapunov and LaSalle's invariance-based analysis is used to prove the stability of the proposed control laws. Experiment results performed on the self-build HILS testbed confirm its superior performance and robustness. Future work will focus on building a quadrotor helicopter with a high-accuracy position sensor, i.e., a D-GPS receiver, and validating the proposed control strategy via outdoor flight experiments.

Appendix A

Definition 1. (Filippov Solution [24]): A function $x : [0, \infty) \to R^n$ is called a solution of $\dot{x} = f(x, t)$ on $[0, \infty)$ if $x(t)$ is absolutely continuous and for almost all $t \in [0, \infty)$

$$\dot{x} \in K[f]\ (x(t), t)$$

where $f : R^n \times R \to R^n$ is Lebesgue measurable and essentially locally bounded, $K[f](x, t)$ is defined as

$$K[f]\,(x(t), t) \equiv \bigcap_{\delta>0} \bigcap_{\mu N=0} \overline{co} f\,(B\,(x(t), \delta) - N, t)$$

and $\cap_{\mu N=0}$ denotes the intersection over all sets N of Lebesgue measurable zero, $\overline{co}$ denotes convex closure, and $B(x, \delta) = \{v \in R|\ \|x(t) - v\| < \delta\}$.

Definition 2. (Clarke's Generalized Gradient [24]): For a function $V: R^n \times [0,\infty) \to R$ that is locally Lipschitz in (x,t), define the generalized gradient of V at (x,t) by

$$\partial V(x,t) = \overline{co}\left\{\lim \nabla V(x,t) | (x_i,t_i) \to (x,t), (x_i,t_i) \notin \Omega_V\right\}$$

where Ω_V is the set of measure zero where the gradient of V is not defined.

Lemma 6. (Chain Rule [24]): Based on the above definitions, let $x(\cdot)$ be a Filippov solution of $\dot{x} = f(x,t)$ and V be a locally Lipschitz regular function. Then, V is absolutely continuous, $(d/dt)V(x(t),t)$ exists almost everywhere (a.e.), i.e., for almost all $t \in [0,\infty)$, and $\dot{V}(x,t) \overset{a.e.}{\in} \tilde{V}(x,t)$, where

$$\dot{\tilde{V}} := \bigcap_{\xi \in \partial V(x,t)} \xi^T \begin{pmatrix} K[f](x(t),t) \\ 1 \end{pmatrix}.$$

APPENDIX B

Proof of Lemma 3: Substituting (8) into f_Δ in (7) yields

$$\|f_\Delta\| = \frac{1}{m} |u_t(E)| \, \|H(E,e)\| \tag{64}$$

where $H(E,e) = [0,0,0,h_1,h_2,h_3]^T$ and the term h_i for $i = 1,2,3$ are given by

$$\begin{cases} h_1 = c\phi s\theta c\psi + s\phi s\psi - (c\phi_d s\theta_d c\psi_d + s\phi_d s\psi_d) \\ h_2 = c\phi s\theta s\psi - s\phi c\psi - (c\phi_d s\theta_d s\psi_d - s\phi_d c\psi_d) \\ h_3 = c\phi c\theta - c\phi_d c\theta_d \end{cases} \tag{65}$$

where $s(\cdot)$ and $c(\cdot)$ are abbreviations of $\sin(\cdot)$ and $\cos(\cdot)$ functions.

Based on (8) and (16), the following inequalities hold:

$$\begin{aligned} |u_t(E)| &= m \, \|g e_3 - k_\chi \chi_2 - \varepsilon \chi_1 - \varphi(\hat{s}+\beta) - \rho\| \\ &\le m \left(g + \|k_\chi\| \|\chi_2\| + \|\varepsilon\| \|\chi_1\| + L(t)\right) \end{aligned} \tag{66}$$

where $L(t) = \|\varphi(\hat{s}+\beta)\| + \|\rho\|$. From Theorem 1, it is clear that $\chi, \zeta \in \mathcal{L}_\infty$, then φ, $(\hat{s}+\beta)$, $\rho \in \mathcal{L}_\infty$, which implies that there exists a positive constant l_d satisfying $L(t) \le l_d$.

To obtain the relationship between E and χ, the following auxiliary matrices $I_a, I_b \in \mathbb{R}^{3\times 6}$ are defined as

$$I_a = \left[O^{3\times 3} \vdots I^{3\times 3}\right] \quad I_b = \left[I^{3\times 3} \vdots O^{3\times 3}\right]. \tag{67}$$

Then, χ can be expressed as

$$\begin{cases} \chi_1 = I_b E \\ \chi_2 = I_a E + \alpha I_b E. \end{cases} \tag{68}$$

From (68), (66) can be further upper bounded as follows:

$$|u_t(E)| \le l_c \left(\frac{m(g+l_d)}{l_c} + \|E\| \right) \tag{69}$$

where $l_c = m \cdot \max\{\|k_\chi\| \|I_a + \alpha I_b\|, \|\varepsilon\| \|I_b\|\}$. Thus, the following inequalities can be obtained:

$$|u_t(E)| \begin{cases} 2l_c \|E\|, & \text{for } \|E\| \ge m(g+l_d) l_c^{-1} \\ 2m(g+l_d), & \text{for } \|E\| < m(g+l_d) l_c^{-1}. \end{cases} \tag{70}$$

Let $r_t = m(g+l_d) l_c^{-1}$ and $k_t = 2l_c$, then the results in (62) holds.

Proof of Lemma 4: Replacing ϕ, θ by $\phi_d + e_\phi$, $\theta_d + e_\theta$ and utilizing the trigonometric function $\cos(a+b) = \cos a - \sin(b/2)\sin(a+(b/2))$, the expression of h_3 can be written as

$$\begin{aligned} h_3 &= c\phi c\theta - c\phi_d c\theta_d \\ &= -s\frac{e_\phi}{2} s\left(\phi_d + \frac{e_\phi}{2}\right) c\phi_d - s\frac{e_\phi}{2} s\left(\phi_d + \frac{e_\phi}{2}\right) c\phi_d \\ &\quad + s\frac{e_\phi}{2} s\left(\phi_d + \frac{e_\phi}{2}\right) s\frac{e_\phi}{2} s\left(\phi_d + \frac{e_\phi}{2}\right) \end{aligned} \tag{71}$$

and it can be further upper bounded as

$$|h_3| \le \left|s\frac{e_\phi}{2}\right| + \left|s\frac{e_\phi}{2}\right| + \left|s\frac{e_\phi}{2}\right| \cdot \left|s\frac{e_\phi}{2}\right| \le \frac{3}{4}\left(|e_\phi| + |e_\phi|\right). \tag{72}$$

Thus, the following inequality can be obtained:

$$h_3^2 \le \frac{9}{16}\left(e_\phi^2 + e_\phi^2 + 2|e_\phi| \, |e_\phi|\right) \le \varsigma_3 \left(e_\phi^2 + e_\phi^2\right) \tag{73}$$

where $\varsigma_3 = 9/8$. Similarly, h_1^2 and h_2^2 can be upper bounded as

$$h_1^2 \le \varsigma_1 \left(e_\phi^2 + e_\phi^2 + e_\psi^2\right) \quad h_2^2 \le \varsigma_2 \left(e_\phi^2 + e_\phi^2 + e_\psi^2\right). \tag{74}$$

Then, the upper bound for the norm of $H(\cdot)$ can be described by the following inequality:

$$\|H(E,r_1)\| = \sqrt{h_1^2 + h_2^2 + h_3^2} \le k_H \|r_1\| \tag{75}$$

where $k_H = \sqrt{\sum_{i=1}^3 \varsigma_i}$.

From Lemma 3 and Lemma 4, the norm of the coupling term f_Δ satisfies the following inequality:

$$\|f_\Delta(E,r_1)\| \le \frac{1}{m} k_t \|E\| k_H \|r_1\| = \kappa\left(\|r_1\|\right) \|E\| \tag{76}$$

where $\kappa(\|r_1\|) = (k_t k_H / m)\|r_1\|$ is a class-$\mathcal{K}$ function, which implies that (59) in Lemma 2 holds.

Proof of Lemma 5: Let $V_s(t) = W(\chi,\zeta)$, from Theorem 1, the following inequality holds:

$$\frac{\partial V_s}{\partial E} f_E(E) = \dot{W}(\chi,\zeta) \le 0 \tag{77}$$

which concludes the result in (60).

Substituting (68) into $V_s(t)$ yields

$$\begin{aligned} V_s &= (I_b E)^T \varepsilon (I_b E) + \left[(I_a + \alpha I_b)E\right]^T \left[(I_a + \alpha I_b)E\right] \\ &\quad + \zeta^T \gamma^{-1} k_\chi^{-1} \zeta \\ &= E^T I_M E + \zeta^T \gamma^{-1} k_\chi^{-1} \zeta \ge E^T I_M E \end{aligned}$$

where $I_M = I_b^T \varepsilon I_b + (I_a + \alpha I_b)^T (I_a + \alpha I_b)$, and the norm of I_M can be calculated as: $\|I_M\| = \sqrt{3(\alpha^2+\varepsilon)^2 + 6\alpha^2 + 3}$.

It is not difficult to show that if a and ε are properly selected, there exists a positive constant c_3 satisfying

$$\left\| \frac{\partial V_s}{\partial E} \right\| \|E\| = 2\|I_M\| \|E\|^2 \le c_3 V_s \tag{78}$$

which implies that (61) in Lemma 2 holds.

REFERENCES

[1] Y. Du, J. Fang, and C. Miao, "Frequency domain system identification of an unmanned helicopter based on adaptive genetic algorithm," *IEEE Trans. Ind. Electron.*, vol. 61, no. 2, pp. 870–881, Feb. 2014.

[2] J. J. Lugo and A. Zell, "Framework for autonomous on-board navigation with the AR. Drone," *J. Intell. Robot. Syst.*, vol. 73, no. 1–4, pp. 401–412, Jan. 2014.

[3] H. Liu, G. Lu, and Y. Zhong, "Robust LQR attitude control of a 3-DOF laboratory helicopter for aggressive maneuvers," *IEEE Trans. Ind. Electron.*, vol. 60, no. 10, pp. 4627–4636, Oct. 2013.

[4] D. Mellinger, M. Shomin, and V. Kumar, "Control of quadrotors for robust perching and landing," in *Proc. Int. Powered Lift Conf.*, 2010, pp. 1–8.

[5] F. Rinaldi, S. Chiesa, and F. Quagliotti, "Linear quadratic control for quadrotors UAVs dynamics and formation flight," *J. Intell. Robot. Syst.*, vol. 70, no. 1–4, pp. 203–220, Apr. 2013.

[6] Y. Fang, P. Wang, N. Sun, and Y. Zhang, "Dynamics analysis and nonlinear control of an offshore boom crane," *IEEE Trans. Ind. Electron.*, vol. 61, no. 1, pp. 414–427, Jan. 2014.

[7] N. Sun, Y. Fang, and X. Zhang, "Energy coupling output feedback control of 4-DOF underactuated cranes with saturated inputs," *Automatica*, vol. 49, no. 5, pp. 1318–1325, May 2013.

[8] H. Ramirez-Rodriguez, V. Parra-Vega, A. Sanchez-Orta, and O. Garcia-Salazar, "Robust backstepping control based on integral sliding modes for tracking of quadrotors," *J. Intell. Robot. Syst.*, vol. 73, no. 1–4, pp. 51–66, Jan. 2014.

[9] E. N. Johnson and S. K. Kannan, "Adaptive trajectory control for autonomous helicopters," *J. Guid., Control, Dynam.*, vol. 28, no. 3, pp. 524–538, May/Jun. 2005.

[10] F. Kendoul, "Nonlinear hierarchical flight controller for unmanned rotorcraft: Design, stability, experiments," *J. Guid., Control, Dynam.*, vol. 32, no. 6, pp. 1954–1958, Nov./Dec. 2009.

[11] Z. T. Dydek, A. M. Annaswamy, and E. Lavretsky, "Adaptive control of quadrotor UAVs: A design trade study with flight evaluations," *IEEE Trans. Control Syst. Technol.*, vol. 21, no. 4, pp. 1400–1406, Jul. 2013.

[12] J. E. Slotine and W. Li, *Applied Nonlinear Control*. Englewood Cliffs, NJ, USA: Prentice-Hall, 1991.

[13] A. Astolfi and R. Ortega, "Immersion and invariance: A new tool for stabilization and adaptive control of nonlinear systems," *IEEE Trans. Autom. Control*, vol. 48, no. 4, pp. 590–606, Apr. 2003.

[14] A. Astolfi, D. Karagiannis, and R. Ortega, *Nonlinear and Adaptive Control With Applications*. Berlin, Germany: Springer-Verlag, 2008.

[15] J. Hu and H. Zhang, "Immersion and invariance based command-filtered adaptive backstepping control of VTOL vehicles," *Automatica*, vol. 49, no. 7, pp. 2160–2167, Jul. 2013.

[16] K. Fujimoto, M. Yokoyama, and Y. Tanabe, "I&I-based adaptive control of a four-rotor mini helicopter," in *Proc. 36th Annu. Conf. IEEE Ind. Electron. Soc.*, Glendale, AZ, USA, Nov. 7–10, 2010, pp. 144–149.

[17] A. Astolfi, R. Ortega, and A. Venkatraman, "A globally exponentially convergent immersion and invariance speed observer for mechanical systems with non-holonomic constraints," *Automatica*, vol. 46, no. 1, pp. 182–189, Jan. 2010.

[18] R. Xu and Ü. Özgüner, "Sliding mode control of a class of underactuated systems," *Automatica*, vol. 44, no. 1, pp. 233–241, Jan. 2008.

[19] B. Xian, D. M. Dawson, M. S. de Queiroz, and J. Chen, "A continuous asymptotic tracking control strategy for uncertain nonlinear systems," *IEEE Trans. Autom. Control*, vol. 49, no. 7, pp. 1206–1211, Jul. 2004.

[20] J. Shin, H. J. Kim, Y. Kim, and W. E. Dixon, "Autonomous flight of the rotorcraft-based UAV using RISE feedback and NN feedforward terms," *IEEE Trans. Control Syst. Technol.*, vol. 20, no. 5, pp. 1392–1399, Sep. 2012.

[21] I. González, S. Salazar, and R. Lozano, "Chattering-free sliding mode altitude control for a quad-rotor aircraft: Real-time application," *J. Intell. Robot. Syst.*, vol. 73, no. 1–4, pp. 137–155, Jan. 2014.

[22] F. Kendoul, Z. Yu, and K. Nonami, "Guidance and nonlinear control system for autonomous flight of minirotorcraft unmanned aerial vehicles," *J. Field Robot.*, vol. 27, no. 3, pp. 311–334, May/Jun. 2010.

[23] E. Altuğ, J. P. Ostrowski, and C. J. Taylor, "Control of a quadrotor helicopter using dual camera visual feedback," *Int. J. Robot. Res.*, vol. 24, no. 5, pp. 329–341, May 2005.

[24] N. Fischer, R. Kamalapurkar, and W. Dixon, "LaSalle-Yoshizawa corollaries for nonsmooth systems," *IEEE Trans. Autom. Control*, vol. 58, no. 9, pp. 2333–2338, Sep. 2013.

[25] R. Sepulchre, M. Jankovic, and P. Kokotovic, *Constructive Nonlinear Control*. New York, NY, USA: Springer-Verlag, 1997.

Bo Zhao received the B.E. degree in automation from Tianjin University, Tianjin, China, in 2010, where he is currently working toward the Ph.D. degree in the School of Electrical Engineering and Automation.

His main research interests include unmanned aerial vehicle systems and nonlinear control of robotic systems.

Bin Xian (S'00–M'04–SM'09) received the B.S. degree in mechanical engineering from Tsinghua University, Beijing, China, in 1996, the M.S. degree in electrical engineering from the Institute of Electrical Engineering, Chinese Academy of Sciences, Beijing, in 2000, and the Ph.D. degree in electrical engineering from Clemson University, Clemson, SC, USA, in 2004.

From 2004 to 2005, he was a Postdoctoral Fellow with the Department of Mechanical Engineering and Materials Science, Duke University, Durham, NC, USA. He is currently a Professor with the School of Electrical Engineering and Automation, Tianjin University, Tianjin, China. His main research interests include nonlinear control of mechatronic systems, autonomous aerial vehicle systems, and robotics.

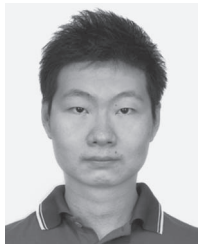

Yao Zhang received the B.S. and M.S. degrees in automation from Tianjin University, Tianjin, China, in 2009, where he is currently working toward the Ph.D. degree in the School of Electrical Engineering and Automation.

His main research interests include nonlinear control, intelligent control, and robotics.

Xu Zhang received the B.S. degree in electrical engineering from Tianjin University, Tianjin, China, in 2006 and the M.S. degree in mechanical engineering from Beijing Institute of Technology, Beijing, China, in 2009. He is currently working toward the Ph.D. degree in the School of Electrical Engineering, Tianjin University.

His main research interests include navigation and control of micro unmanned helicopters and sensor fusing.